surfaces

MDPI

Article

Selective Chemical Filters for VOF_3: Tailoring MgF_2 Filter Selectivity through Surface Chemistry

Laurent Jouffret [1,*], Jean-Michel Hiltbrunner [2,3], Elodie Petit [1], Ania Selmi [3], Bertrand Morel [3] and Marc Dubois [2]

1 Institut de Chimie de Clermont-Ferrand, CNRS, Université Clermont Auvergne, F-63000 Clermont-Ferrand, France; elodie.petit@uca.fr
2 Clermont Auvergne INP, Université Clermont Auvergne, CNRS UMR6296, 24 Av. Blaise Pascal, F-63178 Aubière, France; jm.hiltbrunner@gmail.com (J.-M.H.); marc.dubois@uca.fr (M.D.)
3 Orano Cycle Tricastin, Hall de Recherche de Pierrelatte, F-26701 Pierrelatte, France; ania.selmi@orano.group (A.S.); bertrand.morel@orano.group (B.M.)
* Correspondence: laurent.jouffret@cnrs.fr

Abstract: In order to synthesize chemical filters for the selective removal of volatile fluorides, commercial magnesium fluoride MgF_2 with high specific surface area (HSA) was investigated. The amount of -OH groups substituting fluorine is not negligible, partly due to the high surface area, but also due to the synthesis route. These hydroxyl groups induce a Lewis basicity on the surface of metal fluorides. The amount of these Lewis basic sites has been tailored using fluorination with F_2 gas. The sorption of VOF_3, used as model gas, onto these fluorides was investigated. The versatility of surface chemistry as a function of a number of Lewis basic sites opens the way to filter selectivity mixture of volatile fluorides depending on their Lewis acidity. HSA MgF_2 acts as a stable matrix towards the gas to be purified, and the selectivity may be achieved by a higher Lewis acidity of the gaseous impurity.

Keywords: high surface area fluoride; chemical filter; volatile fluoride; gaseous fluorination; MgF_2

Citation: Jouffret, L.; Hiltbrunner, J.-M.; Petit, E.; Selmi, A.; Morel, B.; Dubois, M. Selective Chemical Filters for VOF_3: Tailoring MgF_2 Filter Selectivity through Surface Chemistry. *Surfaces* **2023**, *6*, 480–492. https://doi.org/10.3390/surfaces6040032

Academic Editor: Aleksey Yerokhin

Received: 22 September 2023
Revised: 30 October 2023
Accepted: 8 November 2023
Published: 19 November 2023

1. Introduction

Volatile fluorides are involved in numerous industrial applications, either as reagents or pollutants. Most of them are Lewis acids and react with a wide variety of compounds; for example, in organic synthesis, gaseous VOF_3 is often used for oxidative coupling of phenolic rings [1]. Due to their ability to release atomic fluorine, volatile fluorides can also be used as fluorinating agents. Nanoparticles, thin films or atomic layers of tungsten and molybdenum metal are synthesized using WF_6 or MoF_6 as precursors [2,3]; metal deposition occurs through the reaction of MF_6 into M plus 3 F_2. A reactant such as Si_2H_6 is used together with MoF_6 to form Mo layers. Dense films of molybdenum oxide may be deposited by plasma-enhanced chemical vapor deposition using mixtures of MoF_6, H_2, and O_2 [4].

When the volatile fluorides are pollutants, however, chemical filters are needed to remove them. The most important application concerns UF_6, which plays a key role in the nuclear industry. UF_6, as a volatile uranium compound, allows uranium enrichment to ^{235}U whatever the process, i.e., gaseous diffusion, centrifugation, or laser excitation. This particular case highlights the necessity for selectivity of the chemical filter. To provide high-purity nuclear fuel, international standards have been established and the quantity of pollutants allowed in nuclear pellets is restricted. Pollutants originate from both uranium ore, the chemical agents used in the conversion process, and/or the fission products of spent uranium. All these elements are fluorinated during the synthesis of UF_6 and their volatility and solubility in UF_6 vary depending on the element [5]. When the volatility of the impurity is close to that of UF_6, its removal is complicated. Selective chemical filters that do not react with UF_6 are thus highly needed. $Ca(OH)_2$, $Mg(OH)_2$, KOH, either separately or in combination, cannot be used because they react easily with UF_6 [6].

Our strategy involves metal fluorides which contain just a small part of basic -OH groups. Considering the reactivity of the volatile fluorides which must be trapped, the criteria for an effective chemical filter are a high surface area, high porosity to increase the interface with the target gas, chemical stability in order to avoid their decomposition, but also enough Lewis basic sites on the surface to react with volatile fluorides as Lewis acids. To reach sufficient selectivity, the surface chemistry or porosity of the filter must be able to match the chemisorption or physisorption of the gas onto the filter surface.

To fulfil these criteria, our choice was to go towards fluorides with high specific surface area (HSA). Usually, such fluorides are obtained via the sol–gel route [7–11] or by microwave-assisted solvothermal synthesis [12–17]. HSA metal fluorides are prepared using metal alkoxides in an organic medium or various solvents and metal precursors in an aqueous-HF medium. The synthesis conditions using microwave-assisted solvothermal routes, i.e., the choice of precursors, solvent, HF concentration and reaction temperature, strongly influence the formation of various networks with different chemical compositions. Magnesium difluoride MgF_2, better known for its catalytic [18,19] and optical properties [20–22], has been selected as a chemical filter based on previous data on the removal of impurities such as fluorides of technetium [23], molybdenum [24], ruthenium, neptunium or plutonium [25].

The presence of weak basic sites was evidenced in MgF_2 prepared by sol–gel [26] and weak basic sites may prevent reaction with UF_6. Basic sites coexist with a large amount of Lewis acid sites, which explains the unique catalytic properties of MgF_2 prepared by sol–gel [8]. F^- and O^{2-} are both intrinsically Lewis bases; however, fluorine atoms reduce the basicity of oxygen atoms. Moreover, the basicity of MgF_2 is much lower than that of MgO. We propose to adapt the OH content in order to reach the selectivity, VOF_3 versus UF_6 for instance, but in a general way by using the Lewis acidity differences of the gases in the mixture. Moreover, the aim is to design a chemical filter that may be regenerated; metal fluoride acts as the support and the OH content changes during reaction with the impurity to be removed.

2. Materials and Methods

2.1. Materials

In order to test the tuning of the OH content, three $MgF_{2-x}(OH)_x$ were used: a commercial MgF_2 received in pellet form (Nippon Puretec, Nagoya, Japan), which is used as either as received or after fluorination treatment, and a locally synthesized oxygen-free MgF_2. The commercial sample was chosen for its ease of use, in pellet rather than powder form, for all the filtering and regeneration operations as well as for the quantities available for future industrial uses. VOF_3 was synthesized locally and used as is.

2.2. Filtering Capacities

All experiments were performed in polytetrafluoroethylene (PTFE) bottles sealed in a nitrogen dry box due to the hygroscopic nature of fluorides. $MgF_{2-x}(OH)_x$ pellets and VOF_3 powders were put in separate nickel baskets. The volatility of VOF_3 at 80 °C allowed the exposure of its gas on $MgF_{2-x}(OH)_x$ samples. After exposure to VOF_3 for 24 h, the $MgF_{2-x}(OH)_x$ pellets were crushed for characterization. The vanadium content on the filter surface was estimated by weight uptake and ICP analysis, both of which gave consistent data.

2.3. Fluorination

Pure molecular fluorine (Solvay, 99%+) was used. A chemical trap filled with soda lime scrubbed F_2 molecules from the exhaust in order to avoid their release into the atmosphere. The gas flow was set at 20 mL·min^{-1}. The treatment was performed at a fluorination temperature T_F = 300 °C. The temperature profile of the treatment is a heating ramp of

$5\ ^\circ C \cdot min^{-1}$, with a stabilization of temperature for 4 h. After this, the reactor was flushed with nitrogen in order to remove all reactive gases.

2.4. Characterization

2.4.1. X-ray Powder Diffraction

X-ray powder diffraction patterns were recorded with a Panalytical X'Pert powder diffractometer in Θ- Θ Bragg Bentano geometry. The samples were transferred to a sealed cell to avoid exposure to moisture, with an aluminum sample holder for some. All patterns were recorded between 5° and 70° in 2Θ with a step of 0.015° and a counting time of 60 min using a back graphite monochromated $CuK\alpha$ radiation ($K\alpha 1$ = 1.54056 Å and $K\alpha 2$ = 1.54439 Å). Profile matching refinements were performed using the FULLPROF software [27].

2.4.2. Adsorption/Desorption Isotherms

The nitrogen adsorption/desorption isotherms were measured using the Micromeritics ASAP 2020 instrument. Prior to each adsorption experiment, the samples were degassed at 473 K under primary vacuum and then under secondary vacuum. Pore volume, specific surface area, and pore size distribution were extracted from the N_2 adsorption/desorption isotherms at 77 K using the BET (Brunauer, Emmett and Teller) and BJH (Barrett, Joyner and Halenda) models for specific surface area (SSA) and pore size distribution for mesoporous materials, respectively.

2.4.3. Raman Spectroscopy

Raman spectra were collected at room temperature using a Bruker RFS 100/S apparatus with a Nd-YAG (aluminum-doped yttrium garnet) laser source at 1064 nm. A total of 500 scans were recorded between 4000 and 25 cm^{-1} Raman shift. Samples were prepared in a sealed fluorinated ethylene-propylene tube (FEP, La Mothe-aux-Aulnais, Saint Gobain) that resulted in the presence of additional Raman bands (marked on the spectra). For the Raman analyses, the MgF_2 single-crystal (Sigma Aldrich, 99%) was used as the reference for oxygen-free magnesium difluoride.

2.4.4. NMR Spectroscopy

Multinuclear ^{19}F, ^{1}H and ^{51}V NMR measurements were carried out with a Bruker Advance Spectrometer with working frequency of 282.2, 300.0 and 78.8 MHz, respectively. A Magic Angle Spinning (MAS) probe operating with 2.5 mm rotors was used allowing a 30 kHz spinning rate. A sequence with a single $\pi/2$ pulse duration of 4.0 µs was used. The ^{19}F, ^{1}H and ^{51}V NMR chemical shifts were externally referenced to $CFCl_3$, tetramethylsilane (TMS) and solution of vanadium phosphate (1 M), respectively.

3. Results and Discussion

3.1. Fluorination to Tailor OH/F Ratio in $MgF_{2-x}(OH)_x$

In order to test the tuning of the OH content, three $MgF_{2-x}(OH)_x$ were used. All the characterizations highlight the presence of -OH groups in the commercial sample, and synthesis via the sol–gel route is strongly suspected. The chemical composition may be written as $MgF_{2-x}(OH)_x$. The aim of post-fluorination of the commercial source is to tailor its OH/F ratio and surface chemistry, but to obtain pure oxygen-free MgF_2, the choice was made to fluorinate an oxygen-free source.

3.1.1. Conversion of MgB_2 into Oxygen-Free MgF_2

In order to select the precursor for the synthesis of oxygen-free MgF_2 via an etching during the fluorination of the element other than Mg, i.e., B, N; Si or P in MgB_2 (BF_3 evolution), Mg_3N_2 (NF_3), Mg_2Si (SiF_4) and Mg_3P_2, the following criteria were used:

1. The expected pore size, in accordance with the size of the released molecules (0.243, 0.320, 0.377 and 0.377 nm) for MgB_2 (BF_3), Mg_3N_2 (NF_3), Mg_2Si (SiF_4) and Mg_3P_2 (PF_5), respectively.
2. The toxicity of the gases released at the completion of the first reaction item.
3. The presence of solid products other than MgF_2.

According to (3) MgC_2 cannot be retained because fluorocarbons may be formed. MgH_2 results after fluorination in the narrowest pores and has not been selected because HF is also undesirable according to (2). A toxic gaseous mixture $S_2F_2/SF_6/F_2$ is also formed from MgS, excluding this precursor according to (2). Mg_3N_2 is not considered because a thermal post-treatment is necessary to remove NH_4F from as-prepared MgF_2, that should lead to decrease the surface area. A narrow pore size being preferred, MgB_2 is selected rather than Mg_3P_2. The fluorination of this MgB_2 precursor at 300 K and 1 atm occurred in two steps: for the addition of F_2 in between 0 and 4 moles, the initial precursor is totally consumed to form solid boron and MgF_2; when F_2 is further added, the boron is then fluorinated as gaseous BF_3. From 4 moles of fluorine gas, the only solid product is MgF_2 and the gaseous mixture consists of BF_3 and F_2. A solid reaction yield slightly higher than 100% is explained by the presence of the intermediate product $Mg(BF_4)_2$ found at the completion of the reaction.

While the XRD pattern of the final product (Figure 1a) reveals only magnesium difluoride MgF_2 [28,29] with traces of MgB_2, the presence of the intermediate product $Mg(BF_4)_2$ is unambiguously revealed by FTIR spectroscopy (Figure 1b) considering the B-F bond vibration bands of at 1111, 1080, 461 cm^{-1} [30].

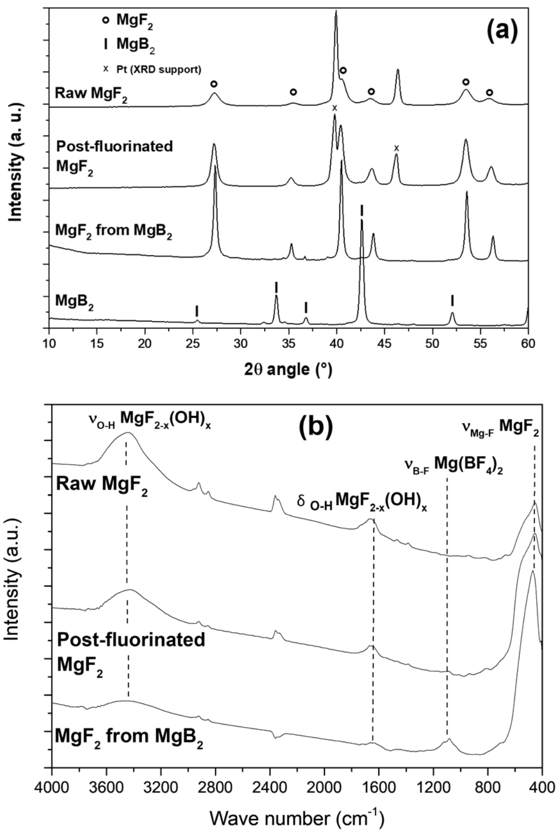

Figure 1. *Cont.*

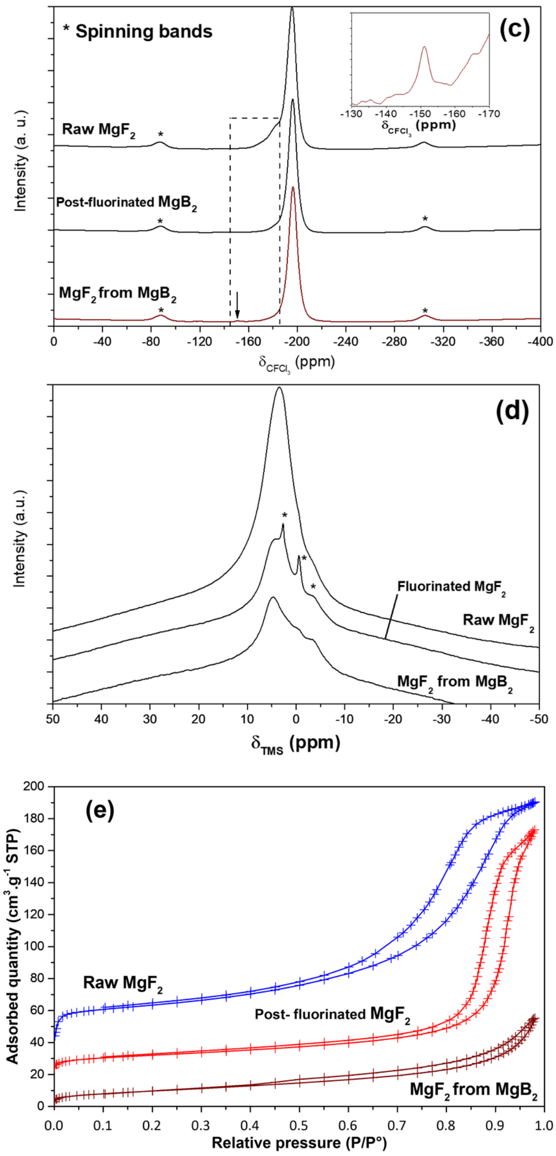

Figure 1. XRD patterns (**a**), FTIR (**b**), MAS 30 kHz ^{19}F (**c**) and ^{1}H (**d**) spectra and N_2 adsorption isotherms (**e**) of raw and post-fluorinated commercial MgF_2 and oxygen-free MgF_2. The (*) marks spinning side bands.

The bands related to the hydroxyl groups (3430 and 1647 cm^{-1}) are absent contrary to the other MgF_2 samples (main peak at 435 cm^{-1} associated with Mg-F vibration mode) [31]. Two bands are identified in the ^{19}F NMR spectrum (Figure 1c). The main band at −196 ppm is assigned to Mg-F bonds. A small shoulder centered at −145 ppm is due to BF_4^- present in very few amounts [32]. BF_4^- reveals the presence of an intermediate compound between MgB_2 and BF_3 following the mechanism:

$$MgB_{2(s,\ black)} \xrightarrow{\Delta,+4F_2} Mg(BF_4)_{2(s)} \xrightarrow{\Delta,-2BF_3} MgF_{2(s,\ white)}$$

It is worthwhile to note that no shoulders indicating the presence of hydroxyl groups are observed in the final product. As a matter of fact, OH groups result in a change in electronic density around the ^{19}F nuclei in their neighboring and consequently a small band should appear at higher chemical shift due to the decrease in the Mg-F bond ionicity (increase in the covalence of the Mg-F bond). A band or shoulder is then observed in the −160/−180 ppm range for other MgF_2 samples; its intensity is related to the synthesis and post-treatment but mainly to the nature and concentration of the hydroxyl groups substituting fluorine. The higher the intensity of this band, the higher the content of hydroxyl groups, (Figure 1c). The ^1H NMR spectrum of MgF_2 without oxygen (Figure 1d) confirms the absence of hydroxyl groups. The objective of preparing oxygen-free MgF_2 is thus reached. The sample obtained by fluorination of the magnesium diboride precursor exhibits a type II profile for the N_2 isotherm (Figure 1e), typical of non-porous or macroporous materials.

The absence of micropores indicates that the lattice is totally rebuilt during the chemical etching and BF_3 evolution. One should note the SSA (specific surface area) of 35 $m^2 \cdot g^{-1}$ for the oxygen-free MgF_2. BF_3 gaseous molecules which are produced during the fluorination of MgB_2 allow a relatively high specific surface area to be maintained, that is unusual with gas/solid fluorination synthesis of fluorides.

3.1.2. Tailoring of OH/F Ratio in Conventional MgF_2

Considering the ^{19}F NMR spectra (Figure 1c), the main band at −196 ppm is assigned to ^{19}F nuclei in the F-Mg-F groups. This chemical shift is in accordance with the literature data [32]. A shoulder also appears for the raw compound and its intensity decreases after post-fluorination treatment. This shoulder is relative to the presence of hydroxyl groups (OH-Mg-F) in MgF_2. As mentioned previously, the position of the band gives information on the fluorine–oxygen environment of magnesium in MgF_2. By fitting the spectra using two Lorentzian lines, the amount of hydroxyl groups is obtained for each compound. The OH/F ratio is 0.14 for raw MgF_2 and 0.04 for the MgF_2 post-fluorinated at 240 °C. The composition of the two samples can be written $MgF_{1.75}(OH)_{0.25}$ and $MgF_{1.925}(OH)_{0.075}$. Regarding ^1H NMR spectra (Figure 1d), only one band is observed (the others being related to the rotor cap) corresponding to the hydroxyl groups in MgF_2. After fluorination, its intensity, i.e., the amount of OH groups, decreases, confirming the efficiency of the treatment in removing OH.

Conversely, oxygen-free MgF_2 exhibits the characteristics of a non-porous or macroporous compound, raw and post-fluorinated MgF_2 present a type IV hysteresis which is typical of a mesoporous material (Figure 1e). The BJH method indicates an average pore size of 8.3 and 20.3 nm for raw and post-fluorinated pellets of commercial MgF_2, respectively. The increase in pore diameter is due to the coalescence phenomenon induced both by the fluorination temperature and by the release of OH groups. It is not possible to extract an average pore diameter using the BJH method for the sample obtained from the boride precursor because the BJH method is only suitable for mesoporous materials. The BET surfaces are 100 and 72 $m^2 \cdot g^{-1}$ for raw and post-fluorinated MgF_2, respectively. The post-fluorination treatment decreases the surface area by substituting fluorine atoms for hydroxyl groups.

3.2. Sorption of VOF_3 in $MgF_{2-x}(OH)_x$

At this step, three different kinds of magnesium difluoride with various contents of OH groups were available for VOF_3 sorption tests: commercial ($MgF_{1.75}(OH)_{0.25}$), post-fluorinated ($MgF_{1.925}(OH)_{0.075}$) and oxygen-free MgF_2 (MgF_2). After exposure to VOF_3, the relative quantity of vanadium trapped was 3.6 w.% for the raw MgF_2, 2.1 w.% for the post-fluorinated sample and 1.3 w.% for the oxygen-free synthesized product. All weight uptakes were confirmed by ICP analysis (Table 1). The higher the OH/F ratio, the higher the sorption rate. The similitudes between the XRD patterns before and after exposure to VOF_3 indicate no new crystalline phase formed nor any change in crystallinity, the width of diffraction peak being the same as that of MgF_2 before the sorption of VOF_3.

The FTIR spectra of the samples (Figure 2a) reacting with vanadium oxyfluoride reveal the occurrence of magnesium—fluorine and vanadium—oxygen bonds. The V=O and V-F stretching bands of vanadium oxyfluoride are identified as raw and treated commercial MgF_2 after sorption at 1000 cm^{-1} (V=O) and 820 cm^{-1} (V-O) on the IR spectra (Figure 2a) [33,34]. The intensities of the vanadium–oxygen vibration bands are higher for raw MgF_2 than for treated MgF_2 in accordance with the amount of vanadium trapped (3.6

and 2.1 w.%, respectively); see Table 1. Only low bands are detected at 1000 cm^{-1} (V=O) and 720 cm^{-1} (V-F) in the case of oxygen-free samples.

Table 1. Weight uptake after VOF_3 sorption experiments.

MgF_2 Treatment	Bulk Weight Uptake (%)	Vanadium Weight Uptake (%)	Vanadium ICP Analysis (%)
Raw	8.7	3.6	3.4
Post-fluorinated at 240 °C	5.1	2.1	2.0
Synthesized from MgB_2	3.1	1.3	1.2

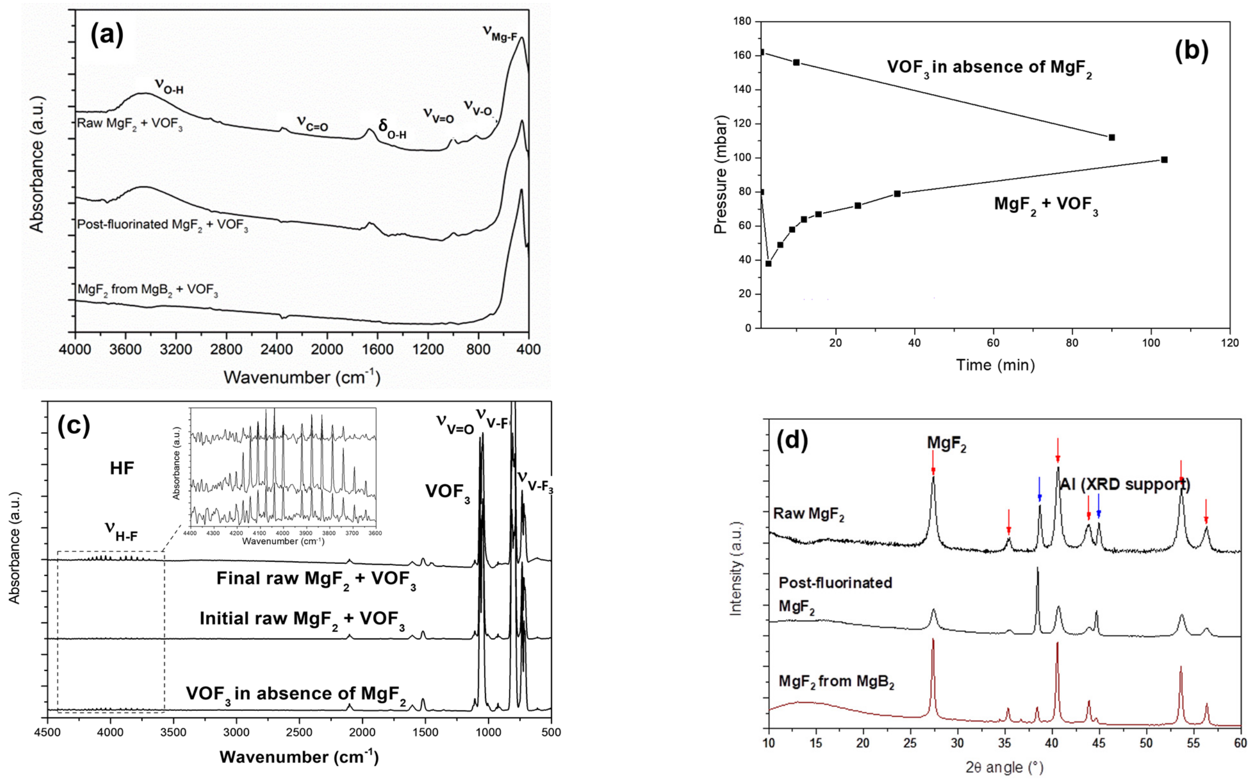

Figure 2. FTIR spectra in the solid (**a**) and gaseous phase (**c**) of adsorbed species by $MgF_{2-x}(OH)_x$ after exposure to VOF_3, evolution of pressure in the gas chamber as a function of time (**b**) and XRD (**d**) patterns of resulting powders.

Gas phase IR and pressure measurements were also performed to follow the nature of the gas generated or consumed during the sorption of VOF_3 on MgF_2. The pressure drops in a first sorption step as expected due to the trapping of VOF_3 molecules onto the surface of the filter, but increases rapidly after, indicating the release of other gases into the IR chamber. The gas-phase FTIR spectra pointed out a massive group of bands between 4500 and 3500 cm^{-1} (Figure 2c). These bands are characteristic of gaseous HF. Their intensity increased during the sorption (Figure 2b).

HF is unambiguously the product of a chemical reaction occurring between $MgF_{2-x}(OH)_x$ and VOF_3. This constitutes another proof of a chemisorption process. V=O and V-F vibration bands characteristic of vanadium oxyfluoride were also detected with Raman spectroscopy (Figure 3).

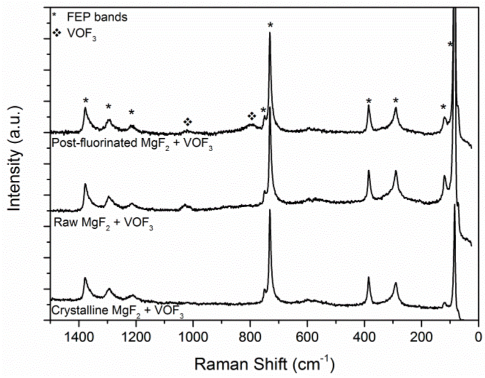

Figure 3. Raman spectra of varied magnesium difluoride samples exposed to VOF_3.

Data from the literature indicate that the first band at 1018 cm^{-1} is assigned to the vibration of the V=O bond in VOF_3 whereas the second at 798 cm^{-1} is related to the V-F bond [35]. As in the FTIR data of MgF_2 exposed to VOF_3, the peak intensity was higher for the raw MgF_2 than for the post-fluorinated sample, once again in accordance with the sorption rates. No bands were observed with the oxygen-free crystalline MgF_2 sample as the quantity of vanadium trapped (close to 1 w.%) was not sufficient to detect any sorption product.

After sorption of VOF_3, the ^{19}F NMR spectra show a single line due to Mg-F bonds (Figure 4a). The shoulder indicating the presence of hydroxyl groups disappears after the sorption. A chemical reaction occurs that removes OH^- groups from the surface of MgF_2 and involves the volatile compound. No further lines due to fluorinated vanadium compounds are observed in the final product. For the ^1H NMR spectra (Figure 4b), the peak intensity assigned to hydroxyl groups in MgF_2 decreases for another contribution at a chemical shift of +9 ppm. This band is assigned to the interaction between vanadium oxyfluoride and protons and confirms the chemical reaction between the OH^- groups and VOF_3. ^{51}V NMR spectra recorded at different spinning rates in order to distinguish between isotropic and spinning bands (Figure 4c) reveal the presence of 3 isotropic bands for raw and post-fluorinated MgF_2 exposed to VOF_3. The isotropic bands at −561, −615 and −791 ppm refer to $VO_2F_2^-$, VOF_3 and VOF_4^-, respectively [36–38].

The presence of $VO_2F_2^-$ ions evidences that VOF_3 reacts with the OH groups on the surface of the chemical filter to form $MgF_{2-x}(VO_2F_2)_x$. Assuming that the vanadium oxyfluoride anion coordinates Mg^{2+} via oxygen and occupies a distorted tetrahedral site, the steric hindrance to hydroxyl groups is radically different and $VO_2F_2^-$ can substitute OH groups only at the surface and not in the rutile network. From an electronic point of view, V^{5+} is a second–order Jahn-Teller ion exhibiting a strong polyhedral distortion. This implies that this molecular species can accommodate a high distortion which permits the stabilization of $MgF_{2-x}(VO_2F_2)_x$ compositions [39].

The generated HF increases the pressure in the reactor and can react with the VOF_3. The resulting product is $HVOF_4$ (trapped on the surface of the filter) in accordance with the isotropic band observed at −791 ppm. As expected, no isotropic band is detected for the oxygen-free MgF_2 because of the low quantity of vanadium trapped. VOF_3 sorption can be summarized as:

$$MgF_{2-x}(OH)_{x(s)} + xVOF_{3(g)} \rightarrow MgF_{2-x}(VO_2F_2)_{x(s)} + xHF_{(g)}$$

In addition to this expected reaction on the metal fluoride surface (chemisorption), a physisorption mechanism may also occur because some of the vanadium is trapped by oxygen-free MgF_2 (1.3 w.%).

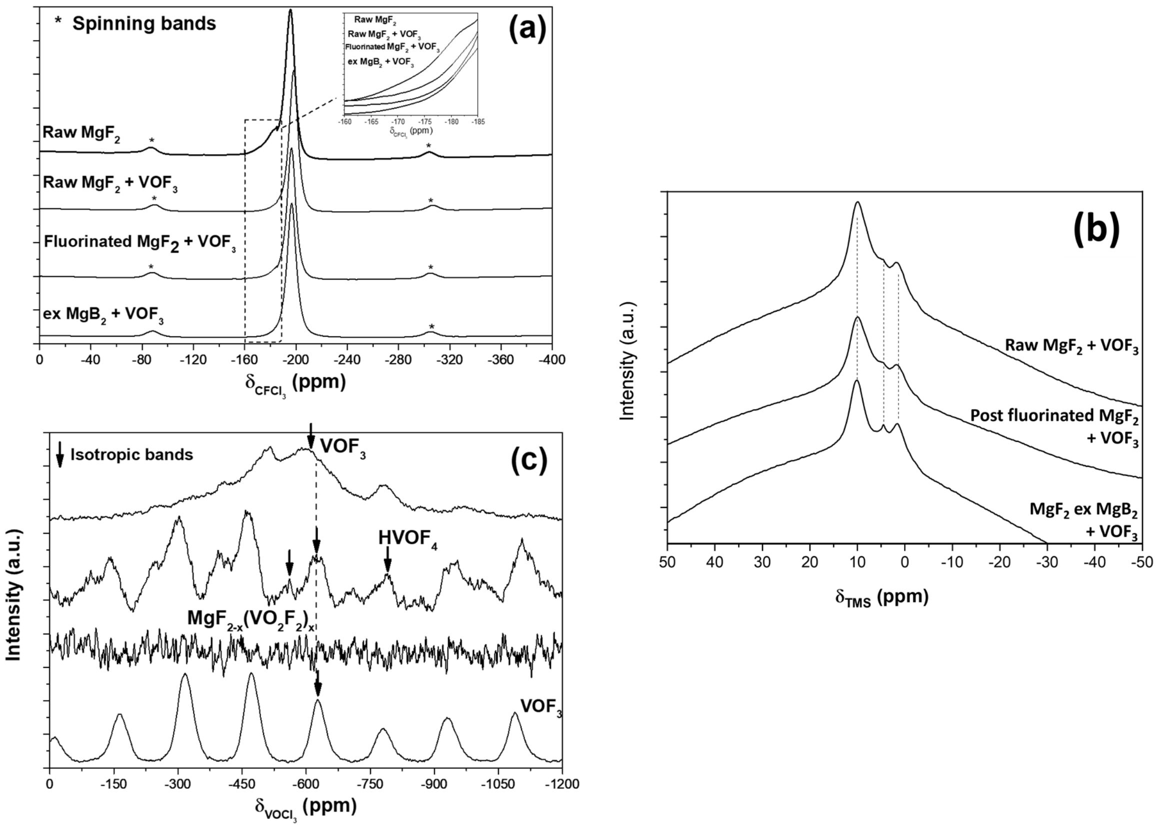

Figure 4. ^{19}F (**a**), ^{1}H (**b**) and ^{51}V (**c**) MAS NMR spectra (spinning rate of 30 kHz) before and after exposure to VOF_3. Arrows mark the isotropic lines.

Chemisorption involves the Lewis basicity of MgF_2 through OH groups. This basicity may be tailored both via the nature, i.e., the coordination number of OH/F anions, the content of OH groups and the cation associated with fluorine. To go further in the discussion, the combination of polarizable cations with low electronegativity (K^+ in $KMgF_3$, Mg^{2+}, Ca^{2+}) and OH^- groups substituting F^- ions is another route to control the strength and number of Lewis basic sites keeping in mind the Lewis acidity of the gas that must be removed. The surface concentration and strength of the Lewis basic sites of the filter can be fitted to the Lewis acidity of the target gas in a gaseous mixture. Considering the structural features of the fluoride series: CaF_2 with a fluorite-type structure and fluorine atoms coordinated fourfold to Ca^{2+}, MgF_2 with a rutile-type structure with fluorine atoms coordinated threefold to Mg^{2+} and $KMgF_3$ with a perovskite-type structure and fluorine atoms twice coordinated to Mg^{2+}, a large variation in the concentration and strength of the Lewis basicity sites is expected. Furthermore, the concentration of OH^- groups can be adjusted by post-fluorination.

3.3. Regeneration of the Chemical Filter

The hydroxyl groups were removed upon exposure to VOF_3 for MgF_2. With the aim to regenerate the chemical filter a two-step process was investigated: the first step consisted of the removal of vanadium with a solvent for V species (cleaning), whereas the second involved a rinsing of the surface. The investigations were performed on a sample with V content of 11,000 ppm after exposure of VOF_3 (ICP data). The extraction rate is given as a function of the cleaning/rinsing agent pair (Figure 5a). A high yield extraction (95%) was achieved with HNO_3 as both cleaning and rinsing agent. It is to note that this removal occurred without significant losses of MgF_2 (only 4 w.%, Figure 5b). After removal of the vanadium, the number of basic sites (OH) must be recovered via the regeneration process. To reach this goal, MgF_2 may be treated with NaOH.

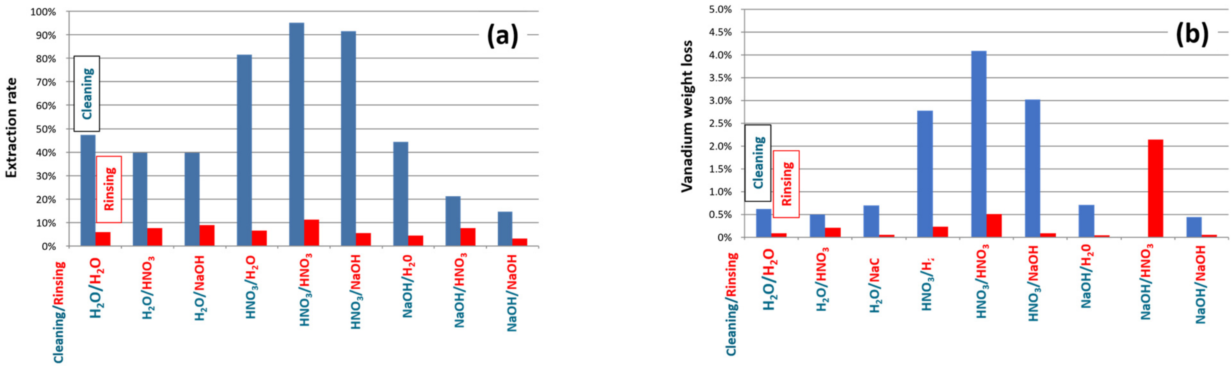

Figure 5. (**a**) Extraction rate of vanadium and (**b**) vanadium weight loss according to the cleaning and rinsing agents.

^{19}F MAS NMR is once again a powerful tool to evidence and quantify the presence of OH groups (Figure 6b) in addition to XRD that proves the unchanged presence of the MgF_2 structure without significant change in $Mg(OH)_2$ (Figure 6a).

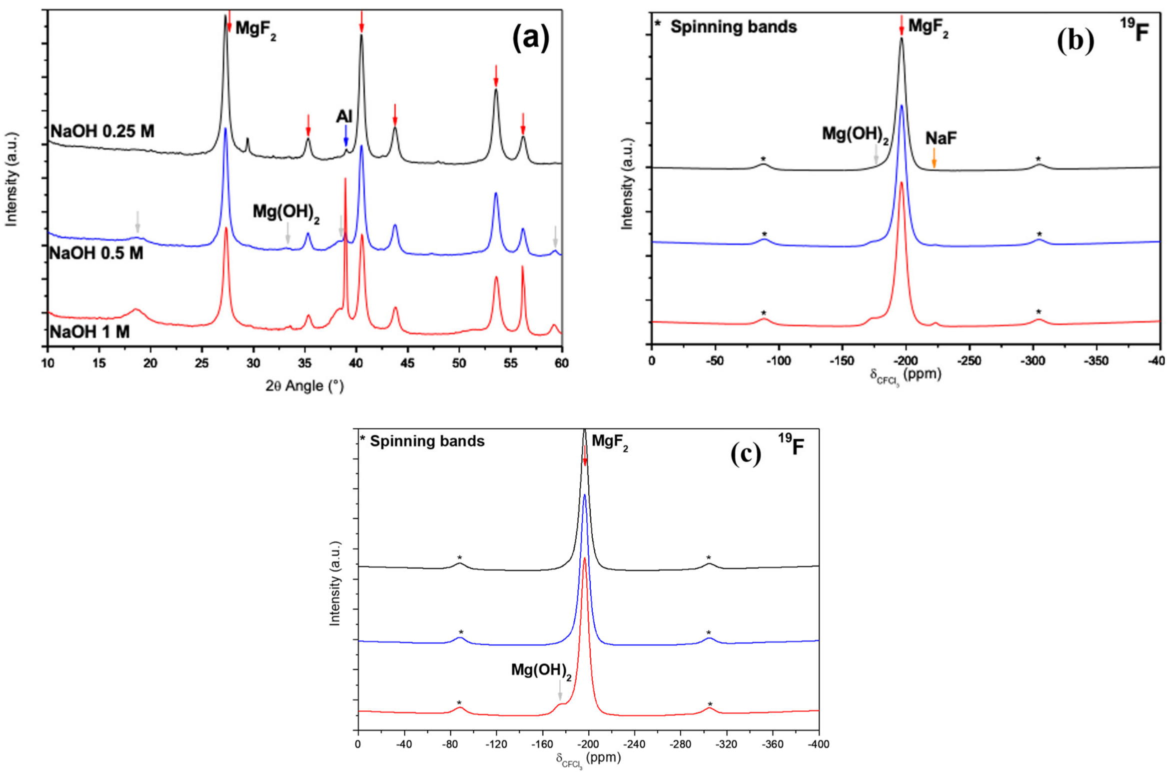

Figure 6. XRD patterns (**a**) and ^{19}F MAS NMR spectra (**b**) of raw MgF_2 treated with NaOH solutions; (**c**) ^{19}F MAS NMR spectra of post-treated MgF_2 exposed to VOF_3, after cleaning (with HNO_3) and rinsing (H_2O) at 60 °C and regeneration with NaOH.

The chemical compositions extracted from the fit of the NMR spectra according to the method described before (Figure 6c) are: $MgF_{1.79}(OH)_{0.21}$, $MgF_{1.72}(OH)_{0.28}$, $MgF_{1.65}(OH)_{0.35}$ as a function of the NaOH concentration, i.e., 0.25, 0.5 and 1 M, respectively. The number of basic sites can then be tailored. In order to nearly recover the initial O/F ratio of 0.25 ($MgF_{1.6}(OH)_{0.4}$), the concentration must be 1 M (O/F = 0.21); the duration of the treatment is 1 h at 60 °C. Two VOF_3 filtering/regeneration cycles were carried out and the change in specific surface area was studied. Table 2 shows the slight decrease in the BET surface after a full filtering/regeneration cycle.

Table 2. Change in the specific surface area during two filtering/regeneration sequences.

	Process Step	Starting Material	After Filtering	After NaOH Regeneration
SSA_{BET} ($m^2 \cdot g^{-1}$)	First run	72	37	64
	Second run	64	38	51

Whereas the specific surface area decreased after the exposure to VOF_3, the initial value was nearly recovered after regeneration with NaOH (1 M concentration, 1 h at 60 °C). Such characteristics prove the possibility of regeneration of the selective filter for both reuse and recovery of vanadium. When the selective filter is used for the purification of UF_6, some uranium species will be present on the surface of the filter; the regeneration aims to remove these species too, underlining its primary importance.

4. Conclusions

Metal fluorides have been investigated as selective chemical filters for the removal of VOF_3, a model gas for volatile fluorides. HSA MgF_2 containing different contents of OH^- groups and an oxygen-free MgF_2 with a rather high specific surface area (35 $m^2 \cdot g^{-1}$) were tested. It is worth noting that such fluorination synthesis using MgB_2 precursor is reported for the first time. The sorption mechanism identified for MgF_2 consists of a chemical reaction between VOF_3 and Lewis basic sites, i.e., OH^- groups. The higher the amount of OH^- groups, the higher the quantity of vanadium trapped. Without hydroxyl groups (free-oxygen MgF_2), physisorption is possible but the amount of vanadium is lower than that of a raw and post-fluorinated commercial MgF_2. It was expected that hydroxyl groups are involved in the reaction with VOF_3 but our data evidence physisorption too. Moreover, understanding the sorption mechanism using complementary techniques allowed us to select the most promising selective and regenerable filter. Both the amounts and strength of the Lewis basic sites may be tailored using a post-fluorination treatment with F_2 gas. This versatility opens the route for the selectivity of filtering for mixtures of volatile fluorides according to the Lewis acidity of the target gas, and the present materials can be considered for active materials of gas sensors [40–42]. Since the reactions with the impurity to be removed occur at the surface of the HSA MgF_2, the metal fluoride matrix is maintained and controlled regeneration of the hydroxyl groups with treatment in NaOH solution is possible.

Author Contributions: Conceptualization, L.J., A.S. and M.D.; methodology, L.J., A.S. and M.D.; investigation, L.J., J.-M.H., E.P. and M.D.; resources, A.S. and B.M.; data curation, L.J. and M.D.; writing—original draft preparation, L.J., J.-M.H. and M.D.; writing—review and editing, L.J. and M.D.; supervision, L.J., A.S., B.M. and M.D.; project administration, L.J. and M.D.; funding acquisition, L.J. and M.D. All authors have read and agreed to the published version of the manuscript.

Funding: This project was undertaken through a University of Clermont Auvergne PhD funded by ORANO Group under a partnership contract with the CNRS.

Data Availability Statement: Data will be made available on request.

Acknowledgments: We thank Alain Demourgues (ICMCB) for valuable discussion about acidity/basicity of fluoride compounds.

Conflicts of Interest: J.-M.H.'s thesis work was funded by ORANO group. A.S. and B.M. work for ORANO group. The funding sponsors had no role in the collection, analyses, or interpretation of data and in the decision to publish the results.

References

1. Langeslay, R.R.; Kaphan, D.M.; Marshall, C.L.; Stair, P.C.; Sattelberger, A.P.; Delferro, M. Catalytic Applications of Vanadium: A Mechanistic Perspective. *Chem. Rev.* **2019**, *119*, 2128–2191. [CrossRef] [PubMed]
2. Landström, L.; Lu, J.; Heszler, P. Size-Distribution and Emission Spectroscopy of W Nanoparticles Generated by Laser-Assisted CVD for Different $WF_6/H_2/Ar$ Mixtures. *J. Phys. Chem. B* **2003**, *107*, 11615–11621. [CrossRef]

3. Seghete, D.; Rayner, G.B., Jr.; Cavanagh, A.S.; Anderson, V.R.; George, S.M. Molybdenum Atomic Layer Deposition Using MoF_6 and Si_2H_6 as the Reactants. *Chem. Mater.* **2011**, *23*, 1668–1678. [CrossRef]
4. Wolden, C.A.; Pickerell, A.; Gawai, T.; Parks, S.; Hensley, J.; Way, J.D. Synthesis of β-Mo_2C Thin Films. *ACS Appl. Mater. Interfaces* **2011**, *3*, 517–521. [CrossRef] [PubMed]
5. Nikolaev, N.S.; Sadikova, A.T. Solubility of fluorides of certain elements in liquid uranium hexafluoride. *Sov. Atom. Energy* **1975**, *39*, 982–987. [CrossRef]
6. Tananaev, I.V.; Nikolaev, N.S.; Luk'yanychev, Y.A.; Opalovskii, A.A. The chemistry of uranium fluorides. *Russ. Chem. Rev.* **1961**, *30*, 654–671. [CrossRef]
7. Kemnitz, E.; Groß, U.; Rüdiger, S.; Shekar, C.S. Amorphous Metal Fluorides with Extraordinary High Surface Areas. *Angew. Chem. Int. Ed.* **2003**, *42*, 4251–4254. [CrossRef]
8. Kemnitz, E.; Groß, U.; Rüdiger, S.; Shekar, C.S. Amorphe Metallfluoride mit außergewöhnlich großer spezifischer Oberfläche. *Angew. Chem.* **2003**, *115*, 4383–4386.
9. Rüdiger, S.; Kemnitz, E. The fluorolytic sol–gel route to metal fluorides—A versatile process opening a variety of application fields. *Dalton Trans.* **2008**, *9*, 1117–1127. [CrossRef]
10. Rüdiger, S.; Eltanamy, G.; Groß, U.; Kemnitz, E. Real sol-gel synthesis of catalytically active aluminium fluoride. *J. Sol-Gel Sci. Technol.* **2007**, *41*, 299–311. [CrossRef]
11. Rüdiger, S.; Groß, U.; Kemnitz, E. Non-aqueous sol–gel synthesis of nano-structured metal fluorides. *J. Fluorine Chem.* **2007**, *128*, 353–368. [CrossRef]
12. Demourgues, A.; Penin, N.; Dambournet, D.; Clarenc, R.; Tressaud, A.; Durand, E. About MX_3 and MX_2 (Mn^+ = Mg^{2+}, Al^{3+}, Ti^{4+}, Fe^{3+}; Xp− = F^-, O^{2-}, OH^-) nanofluorides. *J. Fluorine Chem.* **2012**, *134*, 35–43. [CrossRef]
13. Dambournet, D.; Demourgues, A.; Martineau, C.; Durand, E.; Majimel, J.; Legein, C.; Buzaré, J.Y.; Fayon, F.; Vimont, A.; Leclerc, H.; et al. Microwave Synthesis of an Aluminum Fluoride Hydrate with Cationic Vacancies: Structure, Thermal Stability, and Acidic Properties. *Chem. Mater.* **2008**, *20*, 7095–7106. [CrossRef]
14. Dambournet, D.; Demourgues, A.; Martineau, C.; Durand, E.; Majimel, J.; Vimont, A.; Leclerc, H.; Lavalley, J.C.; Daturi, M.; Legein, C.; et al. Structural investigations and acidic properties of high surface area pyrochlore aluminium hydroxyfluoride. *J. Mater. Chem.* **2008**, *18*, 2483–2492. [CrossRef]
15. Dambournet, D.; Demourgues, A.; Martineau, C.; Majimel, J.; Feist, M.; Legein, C.; Buzaré, J.Y.; Fayon, F.; Tressaud, A. Nanostructured Al-based Fluoride-Oxide Materials with a Core-Shell Morphology. *J. Phys. Chem. C* **2008**, *112*, 12374–12380. [CrossRef]
16. Dambournet, D.; Eltanamy, G.; Vimont, A.; Lavalley, J.C.; Goupil, J.M.; Demourgues, A.; Durand, E.; Majimel, J.; Rüdiger, S.; Kemnitz, E.; et al. Coupling sol-gel synthesis and microwave-assisted techniques: A new route from amorphous to crystalline high-surface-area aluminium fluoride. *Chem. Eur. J.* **2008**, *14*, 6205–6212. [CrossRef]
17. Dambournet, D.; Demourgues, A.; Martineau, C.; Pechev, S.; Lhoste, J.; Majimel, J.; Vimont, A.; Lavalley, J.C.; Legein, C.; Buzaré, J.Y.; et al. Nanostructured Aluminium Hydroxyfluorides Derived from β-AlF_3. *Chem. Mater.* **2008**, *20*, 1459–1469. [CrossRef]
18. Wojciechchova, M.; Zielinski, M.; Pietrowski, M. MgF_2 as a non-conventional catalyst support. *J. Fluorine Chem.* **2003**, *120*, 1–11. [CrossRef]
19. Wang, Y.; Gohari-Bajestani, Z.; Lhoste, J.; Auguste, S.; Hémon-Ribaud, A.; Body, M.; Legein, C.; Maisonneuve, V.; Guiet, A.; Brunet, S. The Effects of Various Parameters of the Microwave-Assisted Solvothermal Synthesis on the Specific Surface Area and Catalytic Performance of MgF_2 Nanoparticles. *Materials* **2020**, *13*, 3566. [CrossRef] [PubMed]
20. Schreiber, H.; Wang, J.; Wilkinson, S.J. Durable MgO–MgF_2 Composite Film for Infrared Anti-Reflection Coatings. European Patent EP2715412, 2012.
21. Lisitsyn, V.M.; Lisitsyna, L.A.; Popov, A.I.; Kotomin, E.A.; Abuova, F.U.; Akilbekov, A.; Maier, J. Stabilization of primary mobile radiation defects in MgF_2 crystals. *Nucl. Instrum. Methods Phys. Res. Sect. B* **2016**, *374*, 24–28. [CrossRef]
22. Cappellini, G.; Furthmüller, J.; Bechstedt, F.; Botti, S. Electronic and Optical Properties of Alkaline Earth Metal Fluoride Crystals with the Inclusion of Many-Body Effects: A Comparative Study on Rutile MgF_2 and Cubic SrF_2. *Symmetry* **2023**, *15*, 539. [CrossRef]
23. Golliher, W.R. Process for Separation and Recovery of Volatile Fluoride Impurities from Uranium Hexafluoride Containing the Same. U.S. Patent 3165376, 12 January 1962.
24. Watanabe, D.; Sasakira, A.; Hoshino, K.; Kawamura, F. Adsorption of molybdenum hexafluoride on magnesium difluoride for uranium purification in FLUOREX reprocessing. *J. Nucl. Sci. Technol.* **2011**, *48*, 1413–1419. [CrossRef]
25. Seregin, M.B.; Mikhalichenko, A.A.; Kuznetsov, A.Y.; Sokovin, G.S.; Chekmarev, A.M. Sorption of gaseous RuF_5 on granulated fluoride sorbents. *Radiochemistry* **2011**, *53*, 288–291. [CrossRef]
26. Wuttke, S.; Vimont, A.; Lavalley, J.-C.; Daturi, M.; Kemnitz, E. Infrared Investigation of the Acid and Basic Properties of a Sol-Gel Prepared MgF_2. *J. Phys. Chem. C* **2010**, *114*, 5113–5120. [CrossRef]
27. Rodriguez-Carvajal, J. Recent advances in magnetic structure determination by neutron powder diffraction. *Phys. B Condens. Matter* **1993**, *192*, 55–69. [CrossRef]
28. Dhaoudadi, H.; Chaabane, H.; Touati, F. Nanorods Synthesized by A Facile. Hydrothermal Method in the Presence of CTAB. *Nano-Micro Lett.* **2011**, *3*, 153–159. [CrossRef]
29. Hunt, G.R.; Perry, C.H.; Ferguson, J. Far-Infrared reflectance and transmittance of Potassium Magnesium fluoride and magnesium fluoride. *Phys. Rev. A* **1964**, *134*, A688–A691. [CrossRef]

30. Heimer, N.E.; Del Sesto, R.E.; Meng, Z.; Wilkes, J.S.; Carper, W.R. Vibrational spectra of imidazolium tetrafluoroborate ionic liquids. *J. Mol. Liq.* **2006**, *124*, 84–95. [CrossRef]
31. Wuttke, S.; Scholtz, G.; Rudiger, S.; Kemnitz, E. Variation of sol-gel synthesis parameters and their consequence for the surface area and structure of magnesium fluoride. *J. Mat. Chem.* **2007**, *17*, 4980–4988. [CrossRef]
32. Scholtz, G.; Stosiek, C.; Noack, J.; Kemnitz, E. Local fluorine environments in nanoscopic magnesium hydr(oxide) fluorides studied by F-19 MAS NMR. *J. Fluor. Chem.* **2011**, *132*, 1079–1085. [CrossRef]
33. Zidan, M.D.; Allaf, A.W. The gas-phase on-line production of vanadium oxytrihalides, VOX_3 and their identification by infrared spectroscopy. *Spectrochim. Acta Part A* **2000**, *56*, 2693–2698. [CrossRef] [PubMed]
34. Beattie, I.R.; Livingston, K.; Reynolds, D.J.; Ozin, G.A. Vibrational spectra of some oxide halides of the transition elements with particular reference to gas-phase and single-crystal Raman spectroscopy. *J. Chem. Soc. A* **1970**, 1210–1216. [CrossRef]
35. Clark, R.J.H.; Rippon, D.M. The vapour phase Raman spectra, Raman band contour analyses, Coriolis constants, force constants, and values for thermodynamic functions of the symmetric top molecules POF_3, $POCl_3$, VOF_3, $VOCl_3$, $PSCl_3$ and $FClO_3$. *Mol. Phys.* **1974**, *28*, 305–319. [CrossRef]
36. Davis, M.F.; Jura, M.; Leung, A.; Levason, W.; Littlefield, B.; Reid, G.; Webster, M. Synthesis, chemistry and structures of complexes of the dioxovanadium(v) halides VO_2F and VO_2Cl. *Dalton Trans.* **2008**, *44*, 6265–6273. [CrossRef] [PubMed]
37. Hibbert, R.C. A ^{51}V and ^{19}F n.m.r. study of vanadium(V) oxide fluoride complexes displaying vanadium–fluorine coupling. *J. Chem. Soc. Chem. Commun.* **1985**, 317–318. [CrossRef]
38. Howell, J.A.S.; Moss, K.C. Nuclear magnetic resonance studies on fluorine-containing compounds. Part III. The tetrafluoro-oxovandate(V) ion. *J. Chem. Soc. A* **1971**, 270–272. [CrossRef]
39. Senchyk, G.A.; Bukhanko, V.O.; Lysenko, A.B.; Krautscheid, H.; Rusanov, E.B.; Chernega, A.N.; Karbowiak, M.; Domasevitch, K.V. AgI/VV Heterobimetallic Frameworks Generated from Novel-Type $\{Ag_2(VO_2F_2)_2(triazole)_4\}$ Secondary Building Blocks: A New Aspect in the Design of SVOF Hybrids. *Inorg. Chem.* **2012**, *51*, 8025–8033. [CrossRef]
40. Chen, C.; Jiang, M.; Luo, X.; Tai, H.; Jiang, Y.; Yang, M.; Xie, G.; Su, Y. Ni-Co-P hollow nanobricks enabled humidity sensor for respiratory analysis and human-machine interfacing. *Sens. Actuators B Chem.* **2022**, *370*, 132441. [CrossRef]
41. Chen, C.; Xie, G.; Dai, J.; Li, W.; Cai, Y.; Li, J.; Zhang, Q.; Tai, H.; Jiang, Y.; Su, Y. Integrated core-shell structured smart textiles for active NO_2 concentration and pressure monitoring. *Nano Energy* **2023**, *116*, 108788. [CrossRef]
42. Zegebreal, L.T.; Tegegne, N.A.; Hone, F.G. Recent progress in hybrid conducting polymers and metal oxide nanocomposite for room-temperature gas sensor applications: A review. *Sens. Actuators A Phys* **2023**, *359*, 114472. [CrossRef]